

PGformer: Proxy-Bridged Game Transformer for Multi-Person Highly Interactive Extreme Motion Prediction

Yanwen Fang^{1,2}, Jintai Chen^{†3}, Peng-Tao Jiang³, Chao Li²,

Yifeng Geng², Eddy K.F. LAM¹, Guodong Li^{†1}

¹The University of Hong Kong, ²DAMO Academy, Alibaba, ³Zhejiang University
 u3545683@connect.hku.hk, jtigerchen@zju.edu.cn, pt.jiang@mail.nankai.edu.cn,
 lllcho.lc@alibaba-inc.com, gengyifeng@gmail.com, hrntlkf@hku.hk, gdli@hku.hk

Abstract

Multi-person motion prediction is a challenging task, especially for real-world scenarios of highly interacted persons. Most previous works have been devoted to studying the case of weak interactions (e.g., walking together), in which typically forecasting each human pose in isolation can still achieve good performances. This paper focuses on collaborative motion prediction for multiple persons with extreme motions and attempts to explore the relationships between the highly interactive persons' pose trajectories. Specifically, a novel cross-query attention (XQA) module is proposed to bilaterally learn the cross-dependencies between the two pose sequences tailored for this situation. A proxy unit is additionally introduced to bridge the involved persons, which cooperates with our proposed XQA module and subtly controls the bidirectional spatial information flows. These designs are then integrated into a Transformer-based architecture and the resulting model is called **Proxy-bridged Game Transformer (PGformer)** for multi-person interactive motion prediction. Its effectiveness has been evaluated on the challenging ExPI dataset, which involves highly interactive actions. Our PGformer consistently outperforms the state-of-the-art methods in both short- and long-term predictions by a large margin. Besides, our approach can also be compatible with the weakly interacted CMU-Mocap and MuPoTS-3D datasets and extended to the case of more than 2 individuals with encouraging results. Our code will be publicly available upon acceptance.

1. Introduction

Human motion prediction aims to forecast a sequence of future 3D motion trajectories given a sequence of past ones, which is widely used in autonomous driving [9, 4],

[†] Corresponding authors.

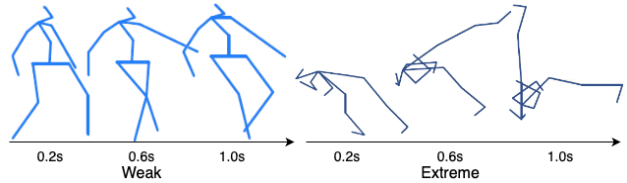


Figure 1. Weakly interacted motions vs highly interacted extreme motions.

target tracking [11], and human-robot interaction [14, 7], *et al.* The skeleton-based human motion sequence is a structured time series, namely, the movement of a single body joint is affected by the coupling of spatial connections with other joints and the temporal trajectory tendency. Therefore, most existing works reformulated motion prediction as a sequence-to-sequence prediction task and tackled this problem by deep learning models [18, 6, 19, 5, 27, 15]. While previous works have achieved remarkable successes, most of them are devoted to exploring single-person prediction which forecasts single human poses in isolation, limiting their direct applications in real-world scenarios of multiple persons. Growing evidence has shown that the motion of one person is typically affected by those of others in a scenario with multiple persons [26]. Recently, multi-person motion prediction has drawn increasing attention from researchers [26, 25, 21]. Even so, these works mainly focused on modeling weakly interacted persons (e.g., hand-shaking and walking together), and yet neglected the scenario of highly correlated persons that is often seen in team sports or collaborative assembly tasks.

To fill this gap, Guo *et al.* [13] collected a new dataset called ExPI (Extreme Pose Interaction) containing human motion sequences in pair with extreme interactions. Based on this dataset, they also proposed a cross-interaction attention (XIA) module and used it before a 26-layer GCN, which is the first work to employ the historical informa-

tion of both people in an interactive fashion. However, their model only exploited the multi-person interactions in the historical poses, predicting the future poses individually without any cross-interaction. To clarify the word ‘extreme’, Figure 1 compares weakly interacted motions and highly interacted extreme motions, showing that the right ones are more complex.

This paper attempts to study the interactions of multiple persons’ pose trajectories with extreme motions from the past to the future, and proposes an end-to-end Transformer-based network for multi-person pose forecasting. Specifically, a novel cross-query attention (XQA) module is first proposed to bilaterally learn the cross-dependencies between the two pose sequences. In our XQA, the two persons’ poses act as queries in computing attention scores to retrieve useful information for each other and share the same attention map. Different from XIA [13], ours can explicitly handle the entire scenario with multiple interacted persons in one step instead of employing two individual attention modules for each person respectively. We use our XQA to learn the cross-interactions between the involved persons’ poses from the past to the future.

To subtly recalibrate the spatial dependencies of the body joints, we further introduce a concept of *proxy* which includes spatial semantic information and interacts with the involved persons in the entire sequence. In addition, we devise two *proxy* units for the past and future poses respectively, and the future one is affected by the past one as well as the future poses in multi-person interactive actions or games. In this way, *proxy* acts as a motion intermediary gathering spatial semantic information entangled in body joints and provides a subtle control of the bidirectional spatial information flows. Cooperating with our XQA, *proxy* facilitates transferring the effective pose information bilaterally between the involved persons from the past to the future, just like a bridge, and thus the future interactions are well modeled. Since this paper builds a Transformer to model the multi-person game (scenario) leveraging an implicitly learnable *proxy*, we call our approach *Proxy-bridged Game Transformer (PGformer)*. Besides, gravity loss for each person is introduced into the loss function, which ensures the center of gravity is kept within a plausible altitude range and avoids a large variance of different models.

Compared with the elaborately designed model of XIA, our PGformer’s architecture stands much closer to currently existing state-of-the-art Transformer-based models, which is much easier to be extended or adapted to other datasets and methods. For instance, there is no need to split different chunks for keys and values separately (like the method in [13]) since PGformer can deal with input sequences of arbitrary length. We evaluate PGformer on the highly interactive ExPI dataset, and experiments show that our model consistently outperforms the state-of-the-art methods both

in short- and long-term predictions. We also show that our approach can be compatible with the weakly interacted CMU-Mocap and MuPoTS-3D datasets and extended to more individuals with encouraging results, validating the generalization ability of our model. To summarize:

- A novel cross-query attention module is proposed to bilaterally learn the cross-dependencies between the two interactive poses, sharing the same attention map.
- A concept of *proxy* is additionally introduced, which cooperates with our XQA to subtly recalibrate the effective pose information in a bidirectional manner.
- We propose a framework called PGformer with the above designs for multi-person highly interactive extreme motion prediction, considering the interactions between the involved persons not only in the historical poses but also in predicting future motions.
- Experiments show that PGformer surpasses the current state-of-the-art methods in both short- and long-term predictions by at least 4–6% on ExPI. We also verify that ours can be compatible with the weakly interacted CMU-Mocap and MuPoTS-3D with more persons.

2. Related Work

Human Motion Prediction. Since human motion prediction (HMP) is a task of spatio-temporal forecasting, recently some researchers used GCN with trainable adjacency matrices to model the pair-wise joint dependencies of human motion [17]. Dang *et al.* [8] further developed GCN-based methods by leveraging multi-scale supervision. Some works employed spatial GCNs and temporal GCNs or spatio-temporal ones to tackle this task [23, 27]. Subsequent methods built upon the success of Transformer-based or attention-based models [24] for long-term motion prediction. For instance, Aksan *et al.* [5] adopted spatial attention and temporal attention separately. Mao *et al.* [16] introduced an attention module before a GCN to capture the similarities between current and historical motion, allowing the model to aggregate past motions for long-term prediction. A non-autoregressive Transformer, supervised by an activity classifier, was leveraged to infer the pose sequences in parallel, avoiding error accumulation [19].

Multi-Person HMP. One key fact is that humans never live in isolation, they continuously interact with other people and objects in real-world scenarios, which means the motion of one person is typically dependent on or correlated with the motion of other people or objects around [26, 13]. With the growing need of scenes with multiple people, some recent works have begun to focus on modeling human-to-human interactions. Mohamed *et al.* [20] employed a

graph-based spatio-temporal model called Social-STGCNN with a specific kernel function in the weighted adjacency matrix to learn the social interactions between pedestrians. TRiPOD [2] used graph attentional networks to model interactions between the involved persons and objects, but applied an RNN with an attentional graph to predict future motion. Wang *et al.* [26] introduced a Transformer-based architecture assisted by a motion discriminator (MRT), and predicted the motion for one person by concatenating other persons’ information in the decoder, which is a straightforward way. TBIFormer [21] utilized a Social Body Interaction Self-Attention (SBI-MSA) module to learn body part dynamics for inter- and intraindividual interactions. Though the works mentioned above aimed at exploring the human-to-human interactions, they only studied the scenes of multiple people with weak interactions and small movements, e.g., moving, standing and chatting.

More recently, Guo *et al.* [13] collected the ExPI dataset and proposed a cross-interaction attention (XIA) mechanism to exploit the historical information of both persons. Nonetheless, only the encoder utilized the XIA module, but the interactions between the future predicted sequences are neglected. Rahman *et al.* [22] concatenated the two involved persons together and sent the features into a spatio-temporal GCN with their proposed initialized weights. However, their model suffered from the problem of instable training and the results had large variances. Besides, the number of persons should be fixed for the model which influences parameters, limiting its broader applications to other datasets with different persons in various scenes. It is worth noting that we have tested the model in [26, 21] on ExPI in our experiments, and the performances suggest that they are insufficient to learn the cross-dependencies between two highly interactive persons.

3. Proposed Method

This section first formulates the problem of multi-person human motion prediction. Then, it proposes a cross-query attention (XQA) module and a *proxy* unit. Lastly, it gives the overall network architecture of our approach.

3.1. Problem Formulation

Given a scene with a pair of persons and their corresponding history motion sequences, our goal is to predict their future 3D motion sequences. Similar to [13], here we use l and f to denote the leader and the follower of two persons to differentiate them. Specifically, given two pose sequences $\mathbf{X}_{1:T}^l = [x_1^l, \dots, x_T^l]$ and $\mathbf{X}_{1:T}^f = [x_1^f, \dots, x_T^f]$ representing history 3D poses with T time steps, we aim to predict the future K poses $\mathbf{X}_{T+1:T+K}^l$ and $\mathbf{X}_{T+1:T+K}^f$. A vector $x_t^l \in \mathbb{R}^{3J}$ containing the Cartesian coordinates of the J skeleton joints is used to repre-

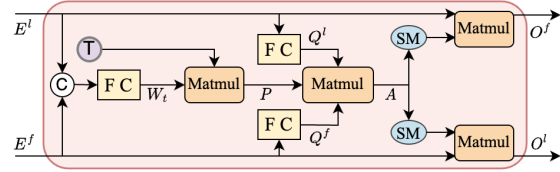


Figure 2. Illustrations of our cross-query attention (XQA) module with a *proxy*, where ‘SM’ and ‘Matmul’ indicate *Softmax* and matrix multiplication. © denotes channel-wise concatenation.

sent the pose of the person l at time step t . This forecasting problem is strongly related to conditional sequence modeling where the goal is to model the joint probability $P(\mathbf{X}_{T+1:T+K}^l, \mathbf{X}_{T+1:T+K}^f | \mathbf{X}_{1:T}^l, \mathbf{X}_{1:T}^f; \theta)$ with model parameters θ . In our work, θ are the parameters of our PG-former. For simplicity, we omit superscript l or f when the superscript variable only represents an arbitrary person, e.g., taking $\mathbf{X}_{1:T}^l$ or $\mathbf{X}_{1:T}^f$ as $\mathbf{X}_{1:T}$.

3.2. Cross-Query Attention Module

Since our goal is to learn two person-specific motion prediction mappings, we propose a cross-query attention (XQA) module to learn the correlations between these two mappings. Our motivation is that the pose trajectory of one person can influence the pose trajectory of the other person since they are highly interactive with each other. The two persons’ pose information should be considered simultaneously for better learning motion properties. Inspired by this, we suppose that the two persons act as queries in computing attention scores to retrieve useful information for each other and share the same attention map. The detailed inner elements of our bidirectional XQA module are given in Figure 2 and can be illustrated as the following.

We denote the output of a Transformer layer (the input of an XQA module) as E^l and $E^f \in \mathbb{R}^{T \times D}$ respectively. Here we omit the subscript for simplicity since the shapes of matrices are all given. Then the queries are given by:

$$Q^l = \text{ReLU}(\text{FC}(E^l)) \quad \text{and} \quad Q^f = \text{ReLU}(\text{FC}(E^f)), \quad (1)$$

where Q^l and $Q^f \in \mathbb{R}^{T \times D}$ are the queries for the two persons’ poses with the model dimension of D , respectively. The shared attention score is built by retrieving query-related information from the other query:

$$A = Q^l [Q^f]^\top, \quad (2)$$

where $A \in \mathbb{R}^{T \times T}$ is the attention map shared by the two interactive persons. As the two persons share the same attention map, we apply the *Softmax* (SM) function along the two different dimensions to obtain the score matrices for them. We utilize the inputs of our XQA module as values for attention directly. In this way, the final outputs are obtained after reweighting the values by the attention score:

$$O^l = \text{SM}(A) \cdot E^f \quad \text{and} \quad O^f = \text{SM}(A^\top) \cdot E^l, \quad (3)$$

where \mathbf{O}^l and \mathbf{O}^f are the outputs of XQA module. Our proposed attention mechanism can be directly extended to a multi-head version. We use $\mathbf{O}^l, \mathbf{O}^f = \text{XQA}(\mathbf{E}^l, \mathbf{E}^f)$ to summarize the above equations (Eq. (1) – (3)) as our XQA module. Besides, our approach can be extended to the case of more than 2 individuals (see details in Section 4.3 and Appendix B.1).

3.3. Proxy

To subtly recalibrate the spatial dependencies of the body joints, we further introduce a concept of *proxy* in the scenario of extreme actions which includes spatial semantic information, and integrate it into our XQA module to bridge the involved persons. The proposed *proxy* unit cooperates with the XQA module and is expected to act as a motion intermediary in the interaction modeling, subtly controlling the bidirectional information flows. The detailed operations to construct a *proxy* are given in the following. Instead of setting *proxy* learnable explicitly, we let it learn and extract the poses’ information from the involved persons in an implicit way. Specifically, M trainable template vectors $t_i \in \mathbb{R}^D (i = 1, \dots, M)$ are first introduced, where M is set very small to control the number of parameters. These learnable vectors constitute the template matrix, denoted as $\mathbf{T} = [t_1, \dots, t_M] \in \mathbb{R}^{M \times D}$, which are used to transform the aggregated spatial features. Then we suppose that the involved persons’ information influences the templates, that is, the mapping of templates is learnt from data. Consequently,

$$\mathbf{W}_t = \text{FC}(\text{Concat}[\mathbf{E}^l, \mathbf{E}^f]), \quad (4)$$

where \mathbf{E}^l and \mathbf{E}^f are the inputs of the XQA module, concatenated by channels. $\mathbf{W}_t \in \mathbb{R}^{T \times M}$ denotes the global spatial features that aggregate the involved persons. Then the proxy is built by transforming the aggregated global spatial information into model dimension and being formulated into spatial dependencies recalibration matrix:

$$\mathbf{P} = \mathbf{T}^\top (\mathbf{W}_t)^\top \mathbf{W}_t \mathbf{T}, \quad (5)$$

where $\mathbf{P} \in \mathbb{R}^{D \times D}$ is the symmetric *proxy* matrix, including the spatial dependencies of the body joints.

Finally, *proxy* is implemented on the cross-query attention since it controls the bidirectional information flows and recalibrates the spatial dependencies:

$$\mathbf{A} = \mathbf{Q}^l \cdot \mathbf{P} \cdot [\mathbf{Q}^f]^\top, \quad (6)$$

where *proxy*, represented as \mathbf{P} , subtly bridges the two queries. It is worth noting that the future *proxy* in the decoder is built by the future templates. Concretely, the future templates used in the decoder \mathbf{T}_{de} can be predicted by the history one used in the encoder \mathbf{T}_{en} :

$$\mathbf{T}_{de} = \text{Attention}(\mathbf{T}_q, \mathbf{T}_{en}, \mathbf{T}_{en}), \quad (7)$$

where $\text{Attention}(\mathbf{Q}, \mathbf{K}, \mathbf{V})$ denotes the attention operation proposed by Vaswani *et al.* [24] with $\mathbf{Q}, \mathbf{K}, \mathbf{V}$ serving as query, key and value matrices, and $\mathbf{T}_q \in \mathbb{R}^{M \times D}$ is the trainable query matrix for future prediction.

3.4. Network Architecture

The overall network architecture of our PGformer is shown in Figure 3. Our PGformer comprises three main components: a pose encoding that embeds the input 3D poses into model dimension, a non-autoregressive Transformer with cross-dependencies learning, and a pose decoding that outputs a sequence of 3D pose vectors. Similar to the vanilla Transformer [24], our PGformer’s encoder and decoder layers are composed of a multi-head attention mechanism (MHA), a feed-forward network (FFN), and a subsequent XQA module with *proxy*, as shown in the left bottom of Figure 3. Following [19], the decoder works in a non-autoregressive fashion to avoid error accumulation and reduce computational cost. As the Transformer learns the temporal dependencies, the model shall identify spatial dependencies between the different body parts in the pose encoding and decoding process. Our approach is trained in a classifier-free and discriminator-free fashion. More specifically, our proposed network architecture works as follows.

PGformer Encoder. We first apply Discrete Cosine Transform (DCT) [3, 17] to encode the input poses $\mathbf{X}_{1:T}$ with temporal smoothness in frequency domain. A fully connected (FC) layer is then used as a pose encoding network to transform the inputs with the dimension of $3J$ into the embeddings (denoted by $\mathbf{E}_{1:T}$) with the model dimension of D . The encoder takes the sequence of pose embeddings added with positional embeddings (PE) as the inputs, which is composed of L layers, each with a Transformer layer (an MHA and an FFN layers) and a subsequent XQA module.

PGformer Decoder. The PGformer decoder takes the encoder outputs (including \mathbf{T}_{en}) as well as a query sequence $\mathbf{Q}_{1:K} = [q_1, \dots, q_K]$ as inputs. It generates the output embeddings through a stack of L PGformer layers, which is the same as in the encoder except for using a different query in the decoder. We adopt the strategy in [13] and let the query q learn from the last M frames of the input sequence $\mathbf{X}_{T-M+1:T}$. Like non-autoregressive Transformer in [19], we use a simple approach to fill $\mathbf{Q}_{1:K}$ using copied entries from q . More precisely, an FC layer and a Conv1D layer are applied to transform the dimension of $\mathbf{X}_{T-M+1:T}$ and squeeze the sequence of length M into one vector $q \in \mathbb{R}^D$. Then each entry q_t in $\mathbf{Q}_{1:K}$ is a copy of q . Lastly, we concatenate the last observation x_T to the decoder outputs and apply a graph convolutional network (GCN) with a residual connection as pose decoding, which treats each joint as a node in a graph to densely learn the spatial relationships between the body joints and transform the outputs of model dimension D back to the original dimension $3J$. To obtain

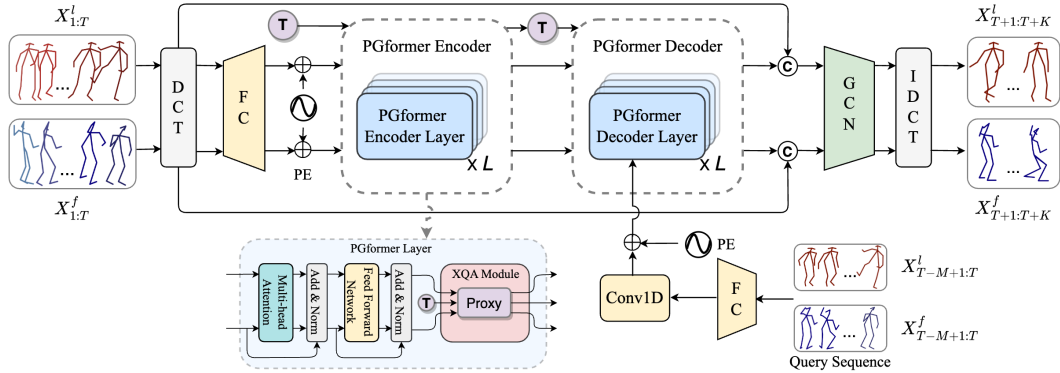


Figure 3. Overview of our PGformer’s architecture for multi-person highly interactive extreme motion prediction. \oplus and \odot represent broadcast element-wise addition and concatenation respectively, and PE means positional encoding. \mathbf{T} denotes the template matrix used to construct *proxy* in the encoder layer, and the *proxy* in the decoder layer is built by the predicted future templates. The left bottom is a schematic diagram of a PGformer layer, including a standard Transformer layer (MHA + FFN) and a subsequent XQA module with *proxy*.

the final predicted poses, the Inverse Discrete Cosine Transform (IDCT) is employed on the outputs of the GCN.

Gravity Loss. In view of forecasting human motion in extreme actions, we propose a gravity loss for each person to ensure the center of gravity is kept within a plausible altitude range and avoid it dramatically vary in contiguous frames. In our experiment, we find that the gravity loss can improve the long-term prediction and control the variances, making the model more stable.

Specifically, we introduce a learnable vector $w \in \mathbb{R}^{J \times 3}$ with length of J and dimension of 3 (the 3D coordinates) for each person to learn the weights of each joint. *Softmax* function is applied to make the summation of J weights for each axis equal to 1. Then the center of gravity at time step t , represented as $g_t \in \mathbb{R}^3$, is computed by:

$$g_t = \sum_{j=1}^J w_j \otimes \hat{x}_{t,j}, \quad (8)$$

where \otimes denotes broadcast element-wise multiplication, and $\hat{x}_{t,j} \in \mathbb{R}^3$ is the predicted pose of joint j at time t . We use offset $\Delta g_t = g_{t+1} - g_t$ between two time steps to represent the variation. Then we take the summation of Δg_t as the gravity loss in the total loss function, which is represented by $\mathcal{L}_{g^l} = \sum_{t=T}^{T+K-1} \Delta g_t^l$ for the leader, and \mathcal{L}_{g^f} is the corresponding gravity loss for the follower.

4. Experiments

In this section, we first experimentally evaluate our approach against other state-of-the-art methods on three benchmarks, including ExPI, CMU-Mocap and MuPoTS-3D datasets. In addition, we evaluate the model qualitatively and conduct ablation studies on ExPI. All models are implemented by PyTorch toolkit on a single V100 GPU. More dataset descriptions, implementation details, experimental results, visualizations and ablation studies are provided in Appendix.

4.1. Datasets

Most of our experiments are based on the challenging ExPI dataset containing highly interactive extreme motions. Besides, our approach is also validated on the CMU-Mocap and MuPoTS-3D datasets with weak interactions to inspect the transferability and the generalization ability.

The Challenging ExPI Dataset. Different from the other multi-person motion datasets, the Extreme Pose Interaction (ExPI) dataset is a special dataset of professional dancers performing Lindy-hop dancing actions, where the two dancers are called leader and follower. The ExPI dataset contains 2 couples of dancers performing 16 extreme actions, and it provides 115 sequences in total, in which each sequence contains 30K frames and 60K instances with annotated 3D body poses and shapes. Each person is recorded at 25 FPS with 3D position of 18 joints. Following the settings in [13], we conduct experiments on the data splits: common action split and unseen action split (see Appendix A.1 for details).

CMU-Mocap and MuPoTS-3D with Weak Interactions. The Carnegie Mellon University Motion Capture Database (CMU-Mocap) [1] provides motion capture recordings from 140 subjects in scenarios of 1 ~ 2 persons, performing various activities. The Multi-person Pose estimation Test Set in 3D (MuPoTS-3D) [10] provides 8,000 annotated frames of poses from 20 real-world scenes, and each sample contains 2 or 3 persons. Different from the ExPI dataset, the interactions between the persons in these two datasets are typically weak (e.g., hand-shaking, standing and chatting). We use the derived CMU-Mocap data (3 persons), MuPoTS-3D data (2–3 persons) and Mix1 (6 persons, blended by CMU-Mocap and MuPoTS-3D) following [21].

4.2. Evaluation Metrics

We adopt the Joint Mean Error (JME) and Aligned Mean Error (AME) in [13] as our evaluation metrics.

Table 1. Results of **JME** (MPJPE) on the common action split with the two evaluation metrics (in *mm*). Lower values mean better performances. The best and second best performances are respectively marked in **bold** and underlined.

Action	A1 A-frame				A2 Around the back				A3 Coochie				A4 Frog classic				A5 Noser				A6 Toss Out				A7 Cartwheel				AVG			
Time (sec)	0.2	0.4	0.6	1.0	0.2	0.4	0.6	1.0	0.2	0.4	0.6	1.0	0.2	0.4	0.6	1.0	0.2	0.4	0.6	1.0	0.2	0.4	0.6	1.0	0.2	0.4	0.6	1.0	0.2	0.4	0.6	1.0
Res-RNN [18]	83	141	182	236	127	224	305	433	99	177	239	350	74	135	182	250	87	152	201	271	93	166	225	321	104	189	269	414	95	169	229	325
LTD [17]	70	125	157	189	131	242	321	426	102	194	260	357	62	117	155	197	72	131	173	231	81	151	200	280	112	223	315	442	90	169	226	303
HRI [16]	52	103	139	188	96	186	256	349	57	118	167	240	45	93	131	180	51	105	149	214	61	125	176	252	71	150	222	333	62	126	177	251
MSR [8]	56	100	<u>132</u>	<u>175</u>	102	187	256	365	65	120	166	244	50	95	127	172	54	100	138	202	70	132	182	258	82	154	218	321	69	127	174	248
SPGSN [15]	68	132	173	245	114	215	272	376	83	155	211	299	63	118	159	209	66	134	182	245	75	148	205	297	95	185	263	388	81	155	209	294
MRT [26]	61	115	143	170	112	202	276	389	83	158	216	324	54	101	136	179	64	121	160	214	71	139	185	261	83	192	280	402	75	147	199	277
TBIFormer [21]	50	100	136	184	94	184	255	346	55	116	163	235	47	95	133	184	50	106	151	217	59	122	172	247	69	147	218	327	61	124	175	249
BP [22]	63	109	140	184	109	193	258	360	69	126	172	247	53	96	129	178	62	111	151	211	73	132	182	261	87	169	238	353	74	134	181	256
XIA [13]	<u>49</u>	<u>98</u>	140	192	84	<u>166</u>	<u>234</u>	<u>346</u>	<u>51</u>	<u>105</u>	<u>154</u>	<u>234</u>	<u>41</u>	<u>84</u>	120	161	43	<u>90</u>	<u>132</u>	<u>197</u>	<u>55</u>	<u>113</u>	<u>163</u>	<u>242</u>	<u>62</u>	<u>130</u>	<u>192</u>	<u>291</u>	<u>55</u>	<u>112</u>	<u>162</u>	<u>238</u>
Ours	46	93	129	173	84	163	230	330	47	99	146	230	39	83	120	161	43	89	130	195	53	107	154	231	59	125	188	286	53	108	156	230

Joint Mean Error (JME). *Joint Mean per joint position Error*, dubbed as JME in short, measures the average L2-norm of different persons in the same coordinate by:

$$\text{JME}(P, G) = \text{MPJPE}(P, G),^1 \quad (9)$$

where P and G are the normalized prediction and ground truth. As our task aims at predicting not only the distinct poses but also the relative position of the two person, P and G are normalized by the same person (e.g., the leader) to keep the information of their related positions. This considers the two interacted persons jointly as a whole and measures both the errors of poses and their relative positions.

Aligned Mean Error (AME). *Aligned Mean per joint position Error* (or aligned MPJPE, AME for short) normalizes the data by removing the global movement of the poses based on a selected root joint (Procrustes analysis [12]) before computing MPJPE. Formally, AME is computed by:

$$\text{AME}(\hat{P}, \hat{G}) = \text{MPJPE}(T_A(\hat{P}, \hat{G}), \hat{G}), \quad (10)$$

where \hat{P} and \hat{G} are the independently normalized poses to erase the errors of the relative positions between the two persons. T_A is a rigid alignment function between the estimated pose and ground truth proposed in [12], further mitigating the impacts of the joints that are used to determine the coordinate (hips and back).

4.3. Implementation Details

Our proposed architecture has L ($L = 4$) PGformer layers in the encoder and decoder with a dimension of D ($D = 128$), and M ($M = 3$) learnable template vectors are used to construct the *proxy*. For training our PGformer on ExPI, we follow the same implementation settings as in [13]. A gravity loss is added to control the variation of center of gravity for each person on the original loss function: $\mathcal{L} = \mathcal{L}_f + 10^{-\epsilon} \mathcal{L}_l + \lambda_l \mathcal{L}_{g^l} + \lambda_f \mathcal{L}_{g^f}$, where \mathcal{L}_f and \mathcal{L}_l are the average MPJPE loss for the leader and follower

¹Mean Per Joint Position Error (MPJPE) calculates the average L2-norm across different joints between the prediction and ground-truth, which is a widely used metric for evaluating 3D pose errors.

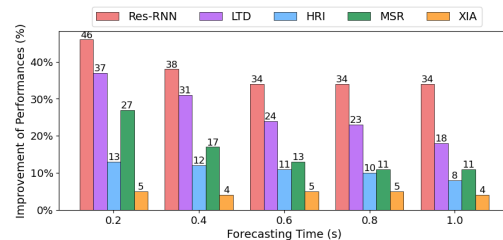


Figure 4. Percentages of improvement of our PGformer compared with other methods at different forecasting time, on the common action split, which are measured by taking the average of the percentages of improvement of average JME and AME error.

respectively, and ϵ denotes epoch index. We set the weights of gravity losses λ_l and λ_f as 0.01 and 0.0001, respectively.

For CMU-Mocap and MuPoTS-3D, the implementation settings exactly follow [26] except that the inputs are absolute coordinates (x_t) instead of motions (Δx_t). The model is trained on a synthesized dataset mixing sampled motions from CMU-Mocap to create 3-person scenes and evaluated on both CMU-Mocap and MuPoTS-3D datasets. In this case, each person is denoted as E^l , and other persons are concatenated by time as E^f (e.g., 3 persons mean 3 pairs of E^l and E^f). This implementation can be adaptive to any number of persons regardless of parameters. The attention score map $A \in \mathbb{R}^{T \times ((n-1) \times T)}$, where n is the number of persons, could still be shared by Q^l and Q^f , but it only be used to obtain O^l for simplicity. The entire process is conducted in an iterative manner over n with the shared parameters (see Appendix B.1 for more details).

4.4. Quantitative Results

4.4.1 Results on ExPI

We compare ours with Res-RNN [18], LTD [17], HRI [16], MSR-GCN (MSR) [8], and XIA-GCN (XIA) [13], of which the results are from [13] in terms of JME and AME in millimeter (*mm*). We also compare ours with SPGSN [15], MRT [26], BestPractices (BP) [22] and TBIFormer [21],

Table 2. Action-wise JME results (in *mm*) on the unseen action split, where the testing actions do not appear in the training.

Action	A8			A9			A10			A11			A12			A13			A14			A15			A16			AVG		
Time (sec)	0.2	0.6	1.0	0.2	0.6	1.0	0.2	0.6	1.0	0.2	0.6	1.0	0.2	0.6	1.0	0.2	0.6	1.0	0.2	0.6	1.0	0.2	0.6	1.0	0.2	0.6	1.0	0.2	0.6	1.0
HRI [16]	57	188	278	49	105	137	55	153	227	80	217	280	68	183	256	45	148	246	93	283	438	61	165	240	49	132	197	62	175	255
MSR [8]	54	177	269	53	123	168	53	150	218	79	221	311	70	190	274	43	148	250	95	278	414	61	174	263	50	142	217	62	177	264
XIA [13]	56	181	274	49	108	139	55	153	222	79	213	282	68	184	260	44	147	243	93	272	410	61	160	230	48	130	193	61	172	250
MRT [26]	57	183	274	50	108	143	54	152	221	79	216	288	69	185	267	45	149	250	94	277	412	61	168	246	49	138	210	62	175	257
TBIFormer [21]	56	179	270	48	106	138	54	153	223	78	210	277	70	188	271	44	148	248	94	279	416	60	164	234	49	136	205	61	174	254
BP [22]	64	190	275	60	127	165	66	162	233	90	232	305	84	212	291	59	156	239	115	293	415	76	189	266	60	151	215	75	190	267
Ours	54	176	265	48	104	136	53	152	220	78	205	260	65	183	256	42	142	220	90	266	408	60	162	232	48	130	191	60	169	243

Table 3. Results of MPJPE on CMU-Mocap and MuPoTS-3D.

Method	CMU-Mocap (3 persons)			MuPoTS-3D (2-3 persons)			Mix1 (6 persons)		
	0.2s	0.6s	1.0s	0.2s	0.6s	1.0s	0.2s	0.6s	1.0s
HRI [16]	49	130	207	81	211	323	51	141	233
MSR [8]	53	146	231	79	222	374	49	132	220
MRT [26]	36	115	192	78	225	349	37	122	212
TBIFormer [21]	30	109	182	66	200	319	34	121	209
Ours	31	108	179	68	197	315	35	120	207

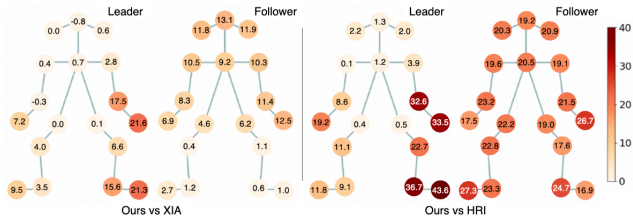


Figure 5. Average performance gains over XIA and HRI of joint-wise JME on ExPI. Darker color means larger performance gains.

whose results are produced by the training protocol of [13].

Common action split. The results on the common action split of ExPI are reported in Table 1. We observe that our proposed PGformer consistently outperforms other methods almost for all actions, in all metrics, in both short- (0.2–0.4 sec) and long-term (0.6–1.0 sec) predictions. Considering the average errors, our PGformer surpasses other state-of-the-art methods in short- and long-term predictions by 4–46% and 4–34% in terms of percentage of improvement on average JME and AME (Figure 4). Even though our model does not achieve the best performances on three actions in long-term forecasting, our approach still obtains the second lowest errors and has comparable performances. Note that, at the horizon of 1.0 sec, for the action of A5/A2, though our model achieves the second-best performance in terms of JME/AME, ours performs the best on the other metric. It is worth noting that MRT [26] and TBIFormer [21] are multi-person-based models proposed on weakly interacted actions, verifying that these methods cannot well model actions with extreme motions.

We also examine the performance gains of ours over XIA and HRI for each joint in Figure 5. As can be seen, our proposed method gets better results almost on all the joints, and larger performance gains are achieved for the joints of limbs. Since joints on the limbs usually have higher motion frequencies, the figure indicates that our PGformer can

better handle high-frequency motions. Comparing ours and XIA on the follower, larger improvements are achieved for joints on the head and shoulder. We reasonably conjecture that the follower has more extreme motions in Lindy-hop dancing actions (see the qualitative results for verification), and our approach can better handle extreme motions.

Unseen action split. The results on the unseen action split are given in Table 2 to measure the generalization ability of models since the testing actions do not appear in the training process. Since the results of the unseen action split in [13] are found to be inconsistent with the forecasting time, we reproduce the compared models and report the results in Table 2. PGformer almost achieves the best and second-best on most of the actions across different forecasting time though the model has never ‘seen’ the testing actions during the training process, verifying our’s generalization ability.

4.4.2 Results on CMU-Mocap and MuPoTS-3D

We additionally evaluate our PGformer on the derived CMU-Mocap, MuPoTS-3D and Mix1 datasets, comparing ours with several state-of-the-art methods, including HRI [16], MSR [8], MRT [26] and TBIFormer [21]. It is worth noting that HRI and MSR are single-person-based methods, while MRT and TBIFormer are multi-person-based methods. Table 3 reports the results in MPJPE at 0.2, 0.6, and 1.0 seconds in the future, and the results of the compared models are from [21]. We can observe that our PGformer and SOTA model TBIFormer perform comparably at different time steps on all datasets, where ours brings more performance gains in long-term prediction. These observations demonstrate that our proposed method can be well generalized to weakly interacted actions and the case of more than 2 individuals.

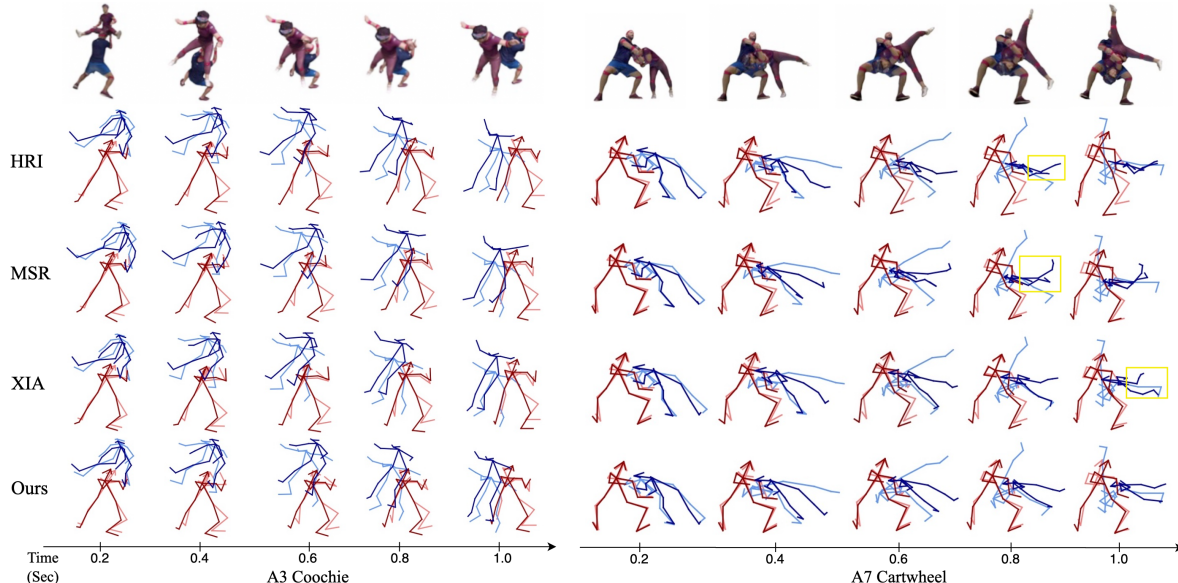


Figure 6. **Qualitative comparisons with other methods.** **1st row:** 3D sample meshes from ExPI Dataset (just for visualization purposes). **2nd-5th rows:** Motion results predicted by HRI [16], MSR-GCN [8], XIA-GCN [13], and our PGformer. Dark red/blue represents the prediction results, while light red/blue indicates the ground truths. Our approach of highly interactive motion prediction achieves significantly better results than other methods. More qualitative examples could be found in Appendix.

4.5. Qualitative Results

Figure 6 shows some qualitative results, comparing our PGformer with HRI, MSR, XIA and the ground truths, on the common action split. It can be seen that our predicted poses are more natural and smoother while being much closer to the ground truths than the other methods. Owing to effectively exploring the interactions between the collaborative persons, our PGformer performs well even on some extreme actions where other methods totally fail. More specifically, see the cases of action A7 in Figure 6, our approach precisely forecasts the actions in long-term prediction while other methods fail to catch the motions. See more in B.4.

4.6. Ablation Study

We ablate different proposed components based on the baseline Transformer (BT) on common actions to identify their roles. The results in Table 4 validate the effectiveness of our proposed *proxy*, XQA module and gravity loss. Remarkably, the XQA module can boost the transformer without interactions notably in long-term prediction, especially on JME, demonstrating our motivation of learning the interactions between the involved persons. Additionally, the gravity loss can improve the long-term prediction and control the variances, making the model more stable. Besides, we also examine the suitability of our suggested baseline Transformer’s architecture, which has 4 PGformer layers in the encoder/decoder with $D = 128$ and $d_{ffn}=1024$ for model dimension and FFN, and 4 heads in MHA with $d_h=64$ for dimension of each head. More ablation study and hyperparameter tunings are given in B.5.

Table 4. Results of JME (MPJPE) for the compared variants. The mean and standard deviation, denoted as avg and std, are computed by 5 runs. BT means the baseline Transformer model. P and Δg_t indicate the *proxy* and gravity loss.

Time (sec)	0.2	0.4	0.6	1.0
PGformer avg (\pm std)	53 (\pm 0.0)	108 (\pm 0.4)	156 (\pm 1.2)	231 (\pm 1.4)
- w/o I/DCT	57	113	161	234
BT avg (\pm std)	54 (\pm 0.5)	112 (\pm 0.5)	166 (\pm 1.8)	247 (\pm 2.2)
+ Δg_t avg (\pm std)	53 (\pm 0.0)	110 (\pm 0.4)	163 (\pm 0.9)	244 (\pm 1.2)
+ XQA	54	110	159	235
+ XQA + P	53	108	157	232
+ XQA + P + Δg_t	53	108	156	231
$D=128, H=4, d_h=32$	54	110	160	238
$D=128, H=8, d_h=32$	53	109	157	233
$D=256, H=8, d_h=32$	53	109	159	237
$D=256, H=8, d_h=64$	53	109	160	239

5. Conclusions

This paper focuses on multi-person pose forecasting in a real-world scenario with highly interactive motions. A simple yet effective Transformer-based framework called PGformer is proposed for multi-person scenario modeling. Specifically, a bespoke XQA module is first proposed to learn the cross-dependencies bidirectionally between the involved persons by a shared attention score map. Since there typically exists a *proxy* continuously affecting the highly interacted persons, a concept of *proxy* is introduced. Cooperating with the XQA module, the *proxy* built by learnable templates can provide a subtle control of the bidirectional information flows from the past to the future, transferring the effective pose information bilaterally like a bridge. The resulting model with the above designs explores the interac-

tions not only in learning the historical poses but in generating the unknown follow-up motions as well. Superior experimental results in both short- and long-term motion predictions on ExPI verify the effectiveness of our PGformer. We also show that our approach can be well-compatible with weakly interacted datasets.

References

- [1] CMU graphics lab motion capture database. [5](#)
- [2] V. Adeli, M. Ehsanpour, I. Reid, J. Niebles, S. Savarese, E. Adeli, and H. Rezatofighi. TRiPOD: Human trajectory and pose dynamics forecasting in the wild. In *2021 IEEE/CVF International Conference on Computer Vision (ICCV)*, pages 13370–13380, Los Alamitos, CA, USA, oct 2021. IEEE Computer Society. [3](#)
- [3] Nasir Ahmed, T Natarajan, and Kamisetty R Rao. Discrete cosine transform. *IEEE transactions on Computers*, 100(1):90–93, 1974. [4](#)
- [4] Ali Akbari, Xien Thomas, and Roozbeh Jafari. Automatic noise estimation and context-enhanced data fusion of IMU and Kinect for human motion measurement. In *International Conference on Wearable and Implantable Body Sensor Networks*, 2017. [1](#)
- [5] Emre Aksan, Manuel Kaufmann, Peng Cao, and Otmar Hilliges. A spatio-temporal Transformer for 3D human motion prediction. In *2021 International Conference on 3D Vision (3DV)*, pages 565–574, 2021. [1](#), [2](#)
- [6] Emre Aksan, Manuel Kaufmann, and Otmar Hilliges. Structured prediction helps 3D human motion modelling. In *The IEEE International Conference on Computer Vision (ICCV)*, Oct 2019. First two authors contributed equally. [1](#)
- [7] Judith Bütepage, Hedvig Kjellström, and Danica Kragic. Anticipating many futures: Online human motion prediction and generation for human-robot interaction. In *2018 IEEE international conference on robotics and automation (ICRA)*, pages 4563–4570. IEEE, 2018. [1](#)
- [8] Lingwei Dang, Yongwei Nie, Chengjiang Long, Qing Zhang, and Guiqing Li. MSR-GCN: Multi-scale residual graph convolution networks for human motion prediction. In *Proceedings of the IEEE/CVF International Conference on Computer Vision*, pages 11467–11476, 2021. [2](#), [6](#), [7](#), [8](#), [13](#), [14](#)
- [9] Nemanja Djuric, Vladan Radosavljevic, et al. Uncertainty-aware short-term motion prediction of traffic actors for autonomous driving. In *WACV*, 2020. [1](#)
- [10] Mehta Dushyant, Sotnychenko Oleksandr, Mueller Franziska, Xu Weipeng, Sridhar Srinath, PonsMoll Gerard, and Theobalt Christian. Single-shot multi-person 3d pose estimation from monocular rgb. In *2018 International Conference on 3D Vision (3DV)*, pages 120–130, Los Alamitos, CA, USA, sep 2018. IEEE Computer Society. [5](#)
- [11] Haifeng Gong, Jack Sim, Maxim Likhachev, and Jianbo Shi. Multi-hypothesis motion planning for visual object tracking. In *2011 International Conference on Computer Vision*, pages 619–626, 2011. [1](#)
- [12] John C Gower. Generalized procrustes analysis. *Psychometrika*, 1975. [6](#)
- [13] Wen Guo, Xiaoyu Bie, Xavier Alameda-Pineda, and Francesc Moreno-Noguer. Multi-person extreme motion prediction. In *Proceedings of the IEEE International Conference on Computer Vision and Pattern Recognition (CVPR)*, 2022. [1](#), [2](#), [3](#), [4](#), [5](#), [6](#), [7](#), [8](#), [12](#), [13](#), [14](#)
- [14] Hema Swetha Koppula and Ashutosh Saxena. Anticipating human activities for reactive robotic response. *2013 IEEE/RSJ International Conference on Intelligent Robots and Systems*, pages 2071–2071, 2013. [1](#)
- [15] Maosen Li, Siheng Chen, Zijing Zhang, Lingxi Xie, Qi Tian, and Ya Zhang. Skeleton-parted graph scattering networks for 3d human motion prediction. In *Proceedings of the european conference on computer vision (ECCV)*, pages 18–36, 2022. [1](#), [6](#)
- [16] Wei Mao, Miaomiao Liu, and Mathieu Salzmann. History repeats itself: Human motion prediction via motion attention. In *European Conference on Computer Vision*, pages 474–489. Springer, 2020. [2](#), [6](#), [7](#), [8](#), [12](#), [13](#), [14](#)
- [17] Wei Mao, Miaomiao Liu, Mathieu Salzmann, and Hongdong Li. Learning trajectory dependencies for human motion prediction. In *Proceedings of the IEEE/CVF International Conference on Computer Vision*, pages 9489–9497, 2019. [2](#), [4](#), [6](#), [14](#)
- [18] Julieta Martinez, Michael J. Black, and Javier Romero. On human motion prediction using recurrent neural networks. In *CVPR*, 2017. [1](#), [6](#), [14](#)
- [19] A. Martínez-González, M. Villamizar, and J.M. Odobez. Pose Transformers (POTR): Human motion prediction with non-autoregressive Transformers. In *IEEE/CVF International Conference on Computer Vision - Workshops (ICCV)*, 2021. [1](#), [2](#), [4](#)
- [20] Abdullah Mohamed, Kun Qian, Mohamed Elhoseiny, and Christian Claudel. Social-STGCNN: A social spatio-temporal graph convolutional neural network for human trajectory prediction. In *Proceedings of the IEEE/CVF Conference on Computer Vision and Pattern Recognition*, pages 14424–14432, 2020. [2](#)
- [21] Xiaogang Peng, Siyuan Mao, and Zizhao Wu. Trajectory-aware body interaction transformer for multi-person pose forecasting. In *Proceedings of the IEEE/CVF Conference on Computer Vision and Pattern Recognition (CVPR)*, pages 17121–17130, June 2023. [1](#), [3](#), [5](#), [6](#), [7](#)
- [22] Muhammad Rameez Ur Rahman, Luca Scofano, Edoardo De Matteis, Alessandro Flaborea, Alessio Sampieri, and Fabio Galasso. Best practices for 2-body pose forecasting. In *CVPRW*, pages 3613–3623, 2023. [3](#), [6](#), [7](#), [13](#)
- [23] Theodoros Sofianos, Alessio Sampieri, Luca Franco, and Fabio Galasso. Space-time-separable graph convolutional network for pose forecasting, 2021. [2](#)
- [24] Ashish Vaswani, Noam Shazeer, Niki Parmar, Jakob Uszkoreit, Llion Jones, Aidan N Gomez, Łukasz Kaiser, and Illia Polosukhin. Attention is all you need. In *Advances in Neural Information Processing Systems*, pages 5998–6008, 2017. [2](#), [4](#)
- [25] Edward Vendrow, Satyajit Kumar, Ehsan Adeli, and Hamid Rezatofighi. SoMoFormer: Multi-person pose forecasting with Transformers, 2022. [1](#)
- [26] Jiashun Wang, Huazhe Xu, Medhini Narasimhan, and Xiaolong Wang. Multi-person 3D motion prediction with multi-range Transformers. In *Advances in Neural Information Processing Systems*, 2021. [1](#), [2](#), [3](#), [6](#), [7](#), [12](#)
- [27] Chongyang Zhong, Lei Hu, Zihao Zhang, Yongjing Ye, and Shi hong Xia. Spatio-temporal gating-adjacency GCN for human motion prediction. *2022 IEEE/CVF Conference on*

Computer Vision and Pattern Recognition (CVPR), pages
6437–6446, 2022. [1](#), [2](#)

Appendix

This appendix contains supplementary explanations and experiments to support our proposed proxy-bridged game Transformer (PGformer). Appendix A supplements the settings for the three datasets, including the descriptions of the ExPI, illustrations for the three splits, and explanations for CMU-Mocap and MuPoTS-3D settings used in our experiments. Appendix B provides more experiment details, results, ablation studies and visualizations.

A. More Information about the Dataset

A.1. ExPI Settings

As described in Section 4.1, 16 actions are recorded in the ExPI dataset, which are split into three data splits: common action split, single action split and unseen action split. Seven of them are common actions (A1–A7), performed by both of the 2 couples. In our experiment, we mainly focus on the common action split and unseen action split.

We use superscript and subscript to denote the couple number and action split respectively, for example, the common action performed by couple 1 is denoted as \mathcal{A}_c^1 . The other nine actions are couple-specific and performed by only one of the couples. The actions A8–A13 in unseen action split are performed by couple 1, denoted as \mathcal{A}_u^1 ; while the actions A14–A16 performed by couple 2 are represented as \mathcal{A}_u^2 .

Common action split. The common actions performed by different couples of actors are considered as training and testing data. Then, training and testing sets contain the same actions but are performed by different persons. In our experiment, following the setting in [13], \mathcal{A}_c^2 is the training set and \mathcal{A}_c^1 is the testing set.

Single action split. In this split, 7 action-wise models are trained independently for each common action by treating the action from couple 2 as the training set and the same action from couple 1 as the corresponding testing set.

Unseen action split. The entire set of common actions including \mathcal{A}_c^1 and \mathcal{A}_c^2 are used as the training set for unseen action split, while the unseen actions $\{\mathcal{A}_u^1, \mathcal{A}_u^2\}$ are used as the testing set. Since the testing actions do not appear in the training process, this unseen action split aims at measuring the generalization ability of models.

A.2. CMU-Mocap and MuPoTS-3D Settings

CMU-Mocap contains a large number of scenes with a single person moving and a small number of scenes with two persons interacting and moving. Wang *et al.* [26] sampled from these two parts and mix them together as their

training data. All the CMU-Mocap data were made to consist of 3 persons in each scene, and the testing set was sampled from CMU-Mocap in a similar way. The generalization ability of the model is evaluated by testing on the MuPoTS-3D (2 – 3 persons) and Mix1 (6 persons) datasets with the model trained on the entire CMU-Mocap dataset.

B. Experiments

B.1. More Implementation Details

ExPI For training our PGformer on ExPI, we follow the same implementation settings as in [13]. Specifically, we predict future motion for 1 second in a recursive manner based on the observed motion of 50 frames. The network is trained by the Adam optimizer with an initial learning rate of 0.005, which is decayed by a rate of $0.1^{1/E}$ (E is the total number of epochs) every epoch. Our model is trained for 40 epochs with a batch size of 32, and the average MPJPE loss is calculated for 10 predicted frames. And we find that XIA-GCN [13] also has to be trained by 40 epochs to achieve the reported results.

CMU-Mocap and MuPoTS-3D The model predicts the future 45 frames (3 s) given 15 frames (1 s) of history as input. All the persons’ pose sequences are forwarded in parallel to the PGformer layers to capture fine relations across themselves and other persons. The gravity loss is not applied to control the center of gravity since the motions in the two datasets are moderate.

Since these two datasets consist of 2–3 persons in each scene, our XQA module should be made adaptive to them. Specifically, each person is denoted as E^l , and other persons are concatenated by time as E^f (e.g., 3 persons mean 3 pairs of E^l and E^f). This implementation can be adaptive to any number of persons regardless of parameters. The attention score map $\mathbf{A} \in \mathbb{R}^{T \times ((n-1) \times T)}$, where n is the number of persons, could still be shared by Q^l and Q^f , but it only be used to obtain O^l for simplicity (O^f is omitted). The entire process is conducted in an iterative manner over n with the shared parameters. Here we just provide a straightforward solution for ≥ 3 extension, and this approach can be easily applied to the scenarios with more than 3 individuals. Instead of squeezing M frames $\mathbf{X}_{T-M+1:T}$ into one vector q , we use the last frame x_t as q directly.

B.2. More Discussions on Quantitative Results

ExPI. We further compare the performance gains of our PGformer with XIA-GCN [13] and HRI [16] for each joint in Figure 5. As can be seen, our proposed method gets better results almost on all the joints, and larger performance gains are achieved for the joints of limbs. Since joints on the limbs usually have higher motion frequencies, the figure indicates that our PGformer can better handle high-frequency

motions. Comparing ours and XIA-GCN on the follower, larger improvements are achieved for joints on the head and shoulder. We reasonably conjecture that the follower has more extreme motions in Lindy-hop dancing actions (see qualitative results for verification), and our approach can better handle extreme motions.

For SPGSN, we apply it adaptively to the ExPI dataset, and decompose the body joints into upper body and lower body following the same spirit as in its experiments on Human3.6M, CMU Mocap and 3DPW datasets.

Though BP [22] is a **contemporaneous work**, we still compare ours with BP on ExPI in Table 5. Since BP used different data and training settings from them used in other models (e.g., XIA, MSR and HRI), we train BP by the training setup provided by ExPI benchmark [13] for fair comparisons. We also train our PGformer by the training settings provided by BP (see the results of BP trained by XIA and PGformer trained by BP). Besides, BP concatenates the joints of the two persons as the nodes of GCN and apply the spatial-temporal GCN, which means the number of persons should be fixed, while our PGformer can be adaptive to different numbers of persons.

Table 5. Results of MPJPE for the compared models. The mean and standard deviation, denoted as avg and std, are computed by 5 runs. We run the code provided by **BP official GitHub** directly and report the results in brackets since it has experiments on ExPI.

Time (sec)	0.2	0.4	0.6	1.0
PGformer avg \pm std	53 \pm 0.0	108 \pm 0.4	156 \pm 1.2	231 \pm 1.4
PGformer (trained by BP)	48	100	149	229
BP-paper (our run)	39 (46)	86 (97)	129 (145)	202 (225)
BP (trained by XIA)	74	134	181	256

B.3. More Comparisons on Quantitative Results

Due to the limited space in main paper, we remove some results of AME in Appendix Table 6. And we provide a more complete percentages of improvement of our PGformer compared with other methods at different forecasting time in Figure 7.

B.4. More Qualitative Results

More qualitative results are provided at the end of this Appendix. We show the examples from each action in Figures 8 to 11. From these examples, with the increase of the forecasting time, the result of our PGformer becomes better than those of other compared methods that independently predict the motions of each person (HRI [16] and MSR-GCN [8]) or only study the interactions between the historical motions (XIA-GCN [13]). For some extreme actions, taking A4 as an example, the poses predicted by MSR-GCN and XIA-GCN at 1 sec forecasting time are weird or look far apart from the ground truths. Nonetheless, our proposed

PGformer successfully predicts the poses which are closer to the ground truths.

B.5. More Ablation Study

We further ablate the pose encoder/decoder of our PGformer, the inner elements of our XQA module with *proxy* and different hyperparameters in Table 7.

The variants with different pose encoding and decoding networks are first compared, and here ‘w/ GCN (enc)’ indicates only using a GCN layer as the pose encoder while using FC layers as the pose decoder. Following the same spirit, our proposed model, which can be denoted as ‘w/ GCN (dec)’, uses an FC layer as the pose encoder and GCNs as the pose decoder. And ‘w/ GCN (both)’ uses GCNs both in the pose encoder and decoder. ‘w/o GCN’ uses FC layers instead of GCNs in the pose encoder and decoder. For all the variants, they use a one-layer encoding network and a four-layer decoding network, which means the numbers of layers in the pose encoding and decoding network are kept the same whether FC layers or GCNs are used. From the ablation results, we can observe that using either FC layers or GCNs as the pose encoding and decoding network has a negligible impact on the performances, but using GCNs as the pose decoder is more suitable. In our experiment, we also find that the pose decoding network with four layers performs better since modeling the relationships of the joints is important for the task of extreme motion prediction.

We then compare the variants with *proxies* combined in different ways, and here $\mathbf{P}' \in \mathbb{R}^{T \times T}$ is given by: $\mathbf{P}' = \mathbf{W}_t \mathbf{T} \mathbf{T}^\top (\mathbf{W}_t)^\top$. The results show that the way in Eq. (6) influencing the bidirectional information performs the best.

Lastly, we ablate the different hyperparameters including the number of templates (M), number of layers and dimensions for model and FFN. From the results, we can find that setting M a small number ($M = 3$ is suggested in our proposed architecture) is sufficient to build *proxy*. From Tables 4 and 7, our suggested architecture has 4 PGformer layers in the encoder/decoder with $D = 128$ and $d_{ffn}=1024$ for model dimension and FFN, and 4 heads in MHA with $d_h=64$ for dimension of each head, which is simpler but more suitable.

Table 6. Results of **AME** on the common action split with the two evaluation metrics (in *mm*). Lower values mean better performances. The best and second best performances are respectively marked in **bold** and underlined.

Action	A1 A-frame	A2 Around the back	A3 Coochie	A4 Frog classic	A5 Noser	A6 Toss Out	A7 Cartwheel	AVG
Time (sec)	0.2 0.4 0.6 1.0	0.2 0.4 0.6 1.0	0.2 0.4 0.6 1.0	0.2 0.4 0.6 1.0	0.2 0.4 0.6 1.0	0.2 0.4 0.6 1.0	0.2 0.4 0.6 1.0	0.2 0.4 0.6 1.0
Res-RNN [18]	59 102 132 167	62 112 152 229	57 102 139 215	48 85 113 157	51 90 120 167	53 94 126 183	74 131 178 265	58 102 137 197
LTD [17]	51 92 116 132	51 91 116 148	43 80 103 130	38 70 89 111	39 70 90 116	42 75 94 123	52 101 139 198	45 83 107 137
HRI [16]	34 69 <u>97</u> 130	44 84 <u>115</u> <u>150</u>	32 65 91 121	27 56 82 112	28 58 85 121	34 66 88 115	42 83 120 171	34 69 97 131
MSR [8]	41 75 99 <u>126</u>	54 96 129 180	41 74 98 135	34 61 82 106	33 59 79 <u>109</u>	42 71 93 124	57 103 146 210	43 77 104 141
XIA [13]	<u>32</u> <u>68</u> 99 128	<u>41</u> <u>82</u> 116 163	<u>29</u> <u>58</u> <u>84</u> <u>116</u>	<u>24</u> 50 73 96	24 <u>51</u> <u>75</u> <u>109</u>	31 <u>62</u> <u>86</u> <u>114</u>	<u>41</u> <u>81</u> <u>115</u> <u>160</u>	<u>32</u> <u>65</u> <u>93</u> <u>127</u>
Ours	31 66 93 120	40 78 109 <u>150</u>	27 54 77 109	23 50 <u>74</u> <u>98</u>	24 49 71 104	31 61 84 112	37 77 111 155	30 62 88 121

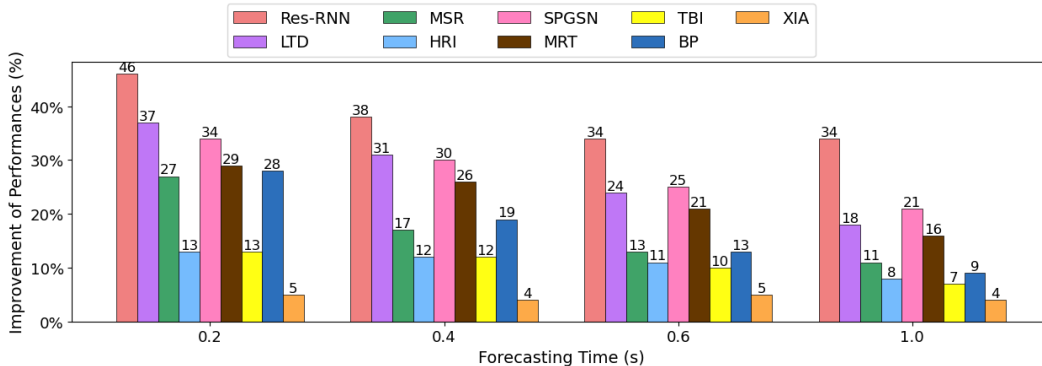


Figure 7. Percentages of improvement of our PGformer compared with other methods at different forecasting time, on the common action split, which are measured by taking the average of the percentages of improvement of average JME and AME error.

Table 7. Ablation study on the pose encoder/decoder, the inner elements of XQA module with *proxy* and different hyperparameters. \otimes and \oplus denote broadcast element-wise multiplication and addition, respectively. d_{ffn} is the hidden dimension of the FFN.

Time (sec)	JME				AME			
	0.2	0.4	0.6	1.0	0.2	0.4	0.6	1.0
Proposed	53	108	156	231	30	62	88	121
w/ GCN (enc)	53	108	157	233	31	63	90	125
w/ GCN (both)	53	108	157	233	31	62	88	122
w/o GCN	53	109	158	234	30	62	88	123
- $\mathbf{A} \otimes \mathbf{P}'$	53	109	159	236	30	62	88	123
- $\mathbf{A} \oplus \mathbf{P}'$	53	110	159	234	31	63	89	123
$M = 8$	53	109	159	236	31	63	90	125
$M = 16$	53	109	158	235	31	62	88	123
3-layer	53	110	159	236	31	63	90	124
6-layer	53	110	161	238	31	63	90	125
$d_{ffn}=512$	54	111	162	240	31	64	92	127
$d_{ffn}=2048$	54	110	161	237	31	63	91	126

potential negative societal impacts include: (1) our approach can be used to synthesize highly realistic human motions, which might lead to the spread of false information; (2) there are still concerns about the invasion of people’s privacy since our approach requires real behavioral information as input, and we are concerned that this may expose the identity information. Nonetheless, on the positive side, our model operates on the processed human skeleton representations instead of the raw data, which contains much less identification information.

Discussion of Limitations. This paper mainly focuses on modeling multi-person extreme actions, while the motions from different actions vary greatly. Hence, it is hard to verify the effectiveness of our PGformer on other extreme actions due to the lack of such datasets. Besides, we only conduct the ablation study on ExPI to decide the architecture of our model. The performances on CMU-Mocap and MuPoTS-3D datasets would be further improved if tuning some hyperparameters.

Ethics Statement. Our original intention for this research is to protect people’s safety in autonomous vehicles, collision avoidance for robotics and surveillance systems. The

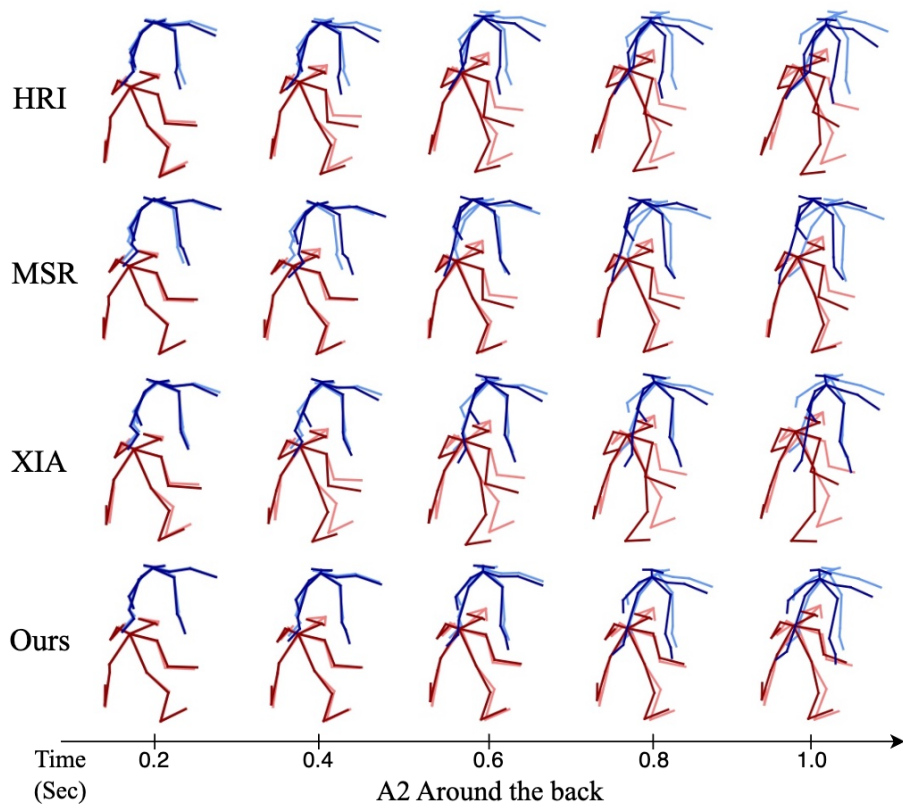
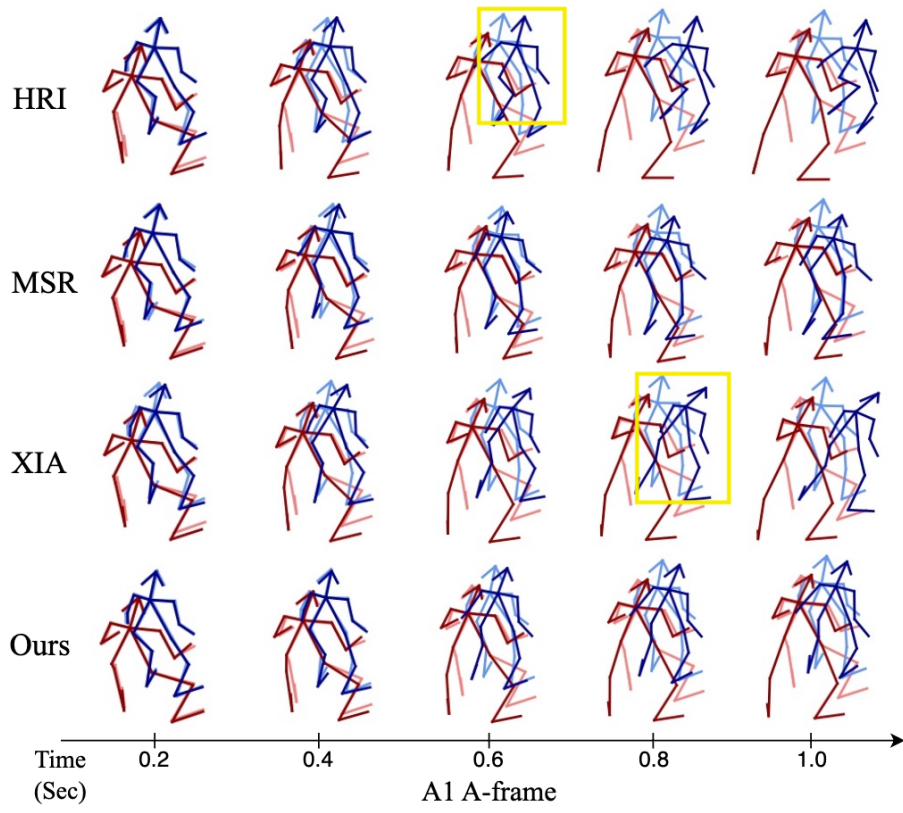


Figure 8. Qualitative results of actions A1 – A2 on the common action split. Dark red/blue represents the prediction results, while light red/blue indicates the ground truths.

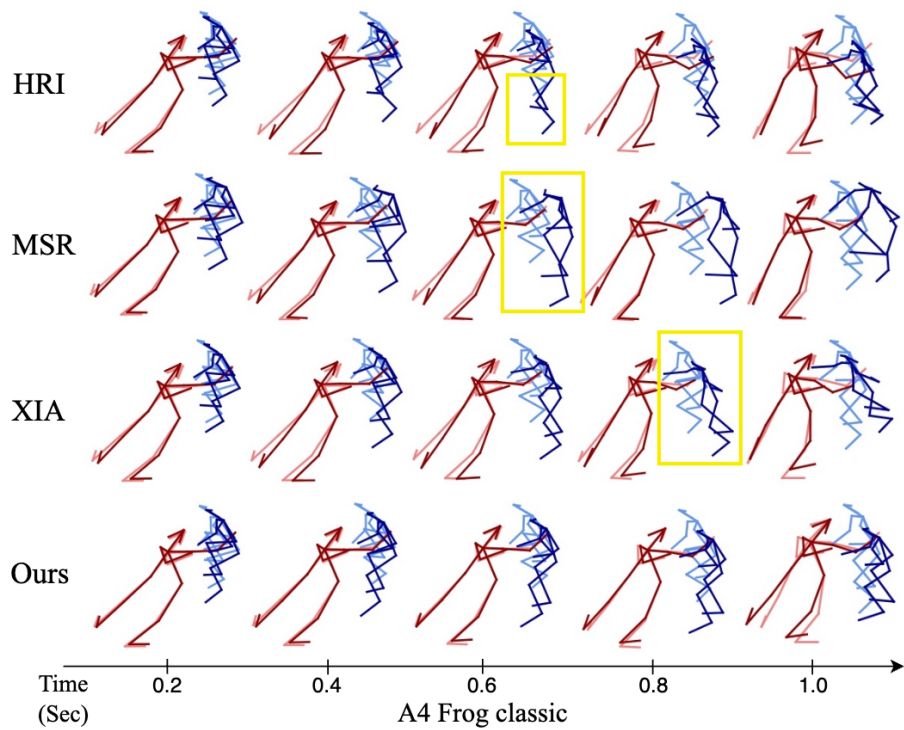
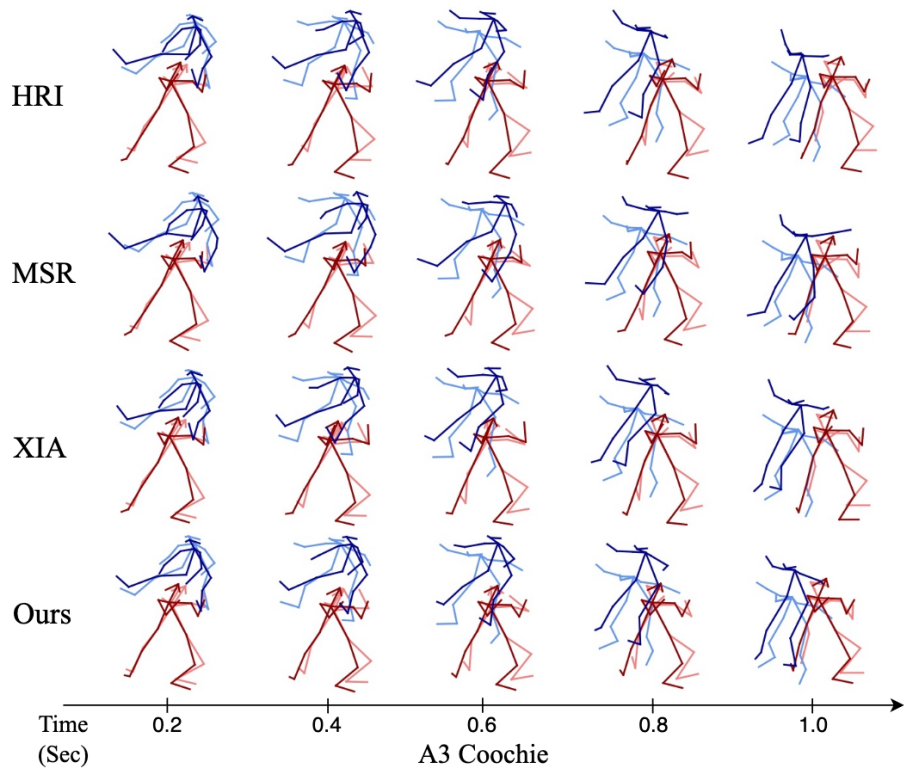


Figure 9. Qualitative results of actions A3 – A4 on the common action split. Dark red/blue represents the prediction results, while light red/blue indicates the ground truths.

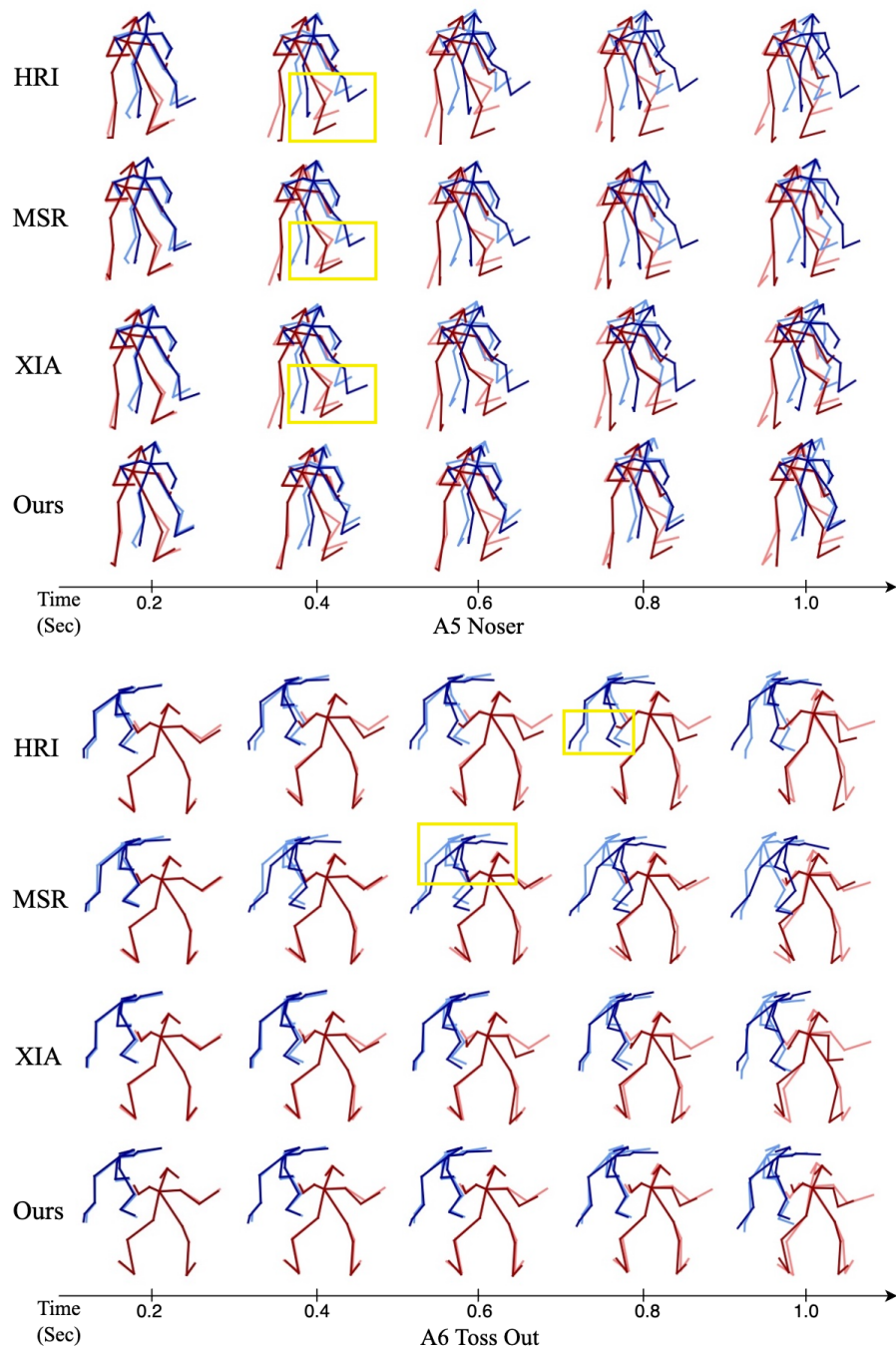


Figure 10. Qualitative results of actions A5 – A6 on the common action split. Dark red/blue represents the prediction results, while light red/blue indicates the ground truths.

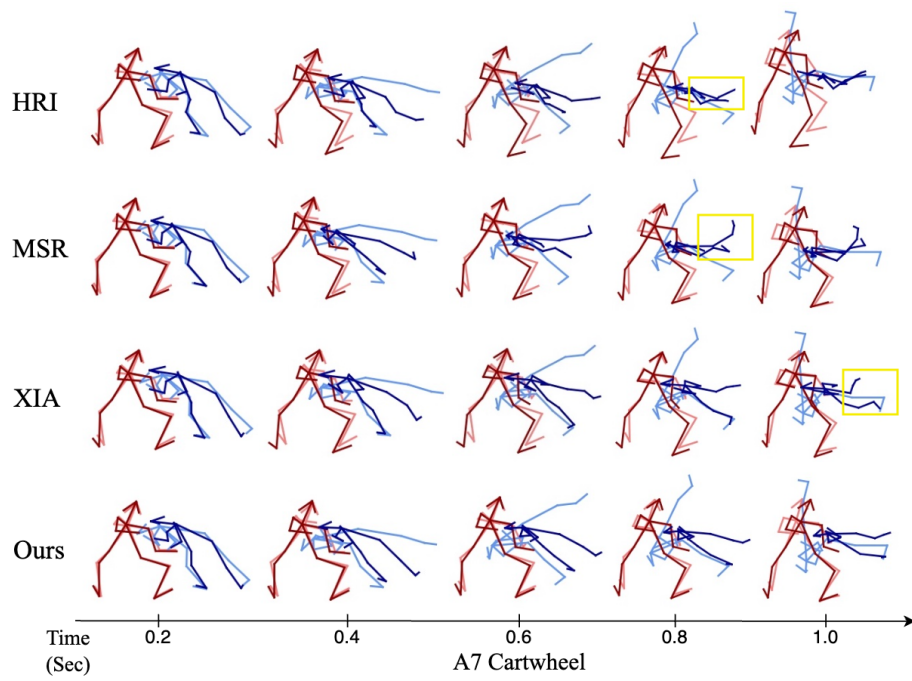


Figure 11. Qualitative results of action A7 on the common action split. Dark red/blue represents the prediction results, while light red/blue indicates the ground truths.